Sychterz, A. and Smith, I.F.C. "Joint Friction during Deployment of a Near-Full-Scale Tensegrity Footbridge" Journal of Structural Engineering, Vol. 143, No. 9, 2017, pp 04017081-1-9 http://cedb.asce.org

Joint friction during deployment of a near-full-scale tensegrity footbridge

Ann C. Sychterz[1] and Ian F. C. Smith[2]

ABSTRACT

Most deployable structures, such as operable roofs and masts, move over one-degree of freedom. This paper describes a structure that involves loosely coupled movement over several degrees of freedom. Analysis models of these structures are typically inaccurate. A source of inaccuracy is joint friction. Static and kinetic friction are studied experimentally and analytically. Simulations have been modified to account for these effects and two methods are used to quantify friction effects. Friction has a significant effect on the movement of the tensegrity structure. Of two candidate parameters, cable tension and interior cable angle, cable angle is the factor that best characterizes friction effects. Values of static and kinetic friction coefficients are not significantly different in this context and this leads to a reduction in the complexity of the friction model for simulation. Including friction effects in analysis decreases the difference between simulations and tests. Lastly, strut elements of the tensegrity structure are most critically affected by friction.

Keywords: Tensegrity structures, friction modeling, deployable structures, full-scale testing

INTRODUCTION

A deployable structure is capable of changing from a compact position to an extended position (Pellegrino 2001). Examples of deployable structures include operable dome roofs,

[1]Ph.D student, S.M.ASCE, Applied Computing and Mechanics Laboratory (IMAC), School of Architecture, Civil and Environmental Engineering (ENAC), Swiss Federal Institute of Technology (EPFL), CH-1015 Lausanne, Switzerland (corresponding author). Email address: ann.sychterz@epfl.ch

[2]Professor, F.ASCE, Applied Computing and Mechanics Laboratory (IMAC), School of Architecture, Civil and Environmental Engineering (ENAC), Swiss Federal Institute of Technology (EPFL), CH-1015 Lausanne, Switzerland

masts, solar arrays, antennas, as well as umbrella-type and tent-type structures. A scissor-like element, bars in an X-shape pinned at their ends and midpoints (Gantes et al. 1989), is an example of a structure that deploys along one degree of freedom. Most structures today are deployed over one degree of freedom. A new generation of structures will deploy over multiple degrees of freedom and this creates a challenge for determining efficient deployment algorithms.

Tensegrity structures are closely-coupled structures that rely on self-stress for stability (Snelson 1996)(Motro 2011)(Pellegrino and Calladine 1986). The 1/4-scale deployable tensegrity structure in this paper is a "hollow-tube" pentagonal shape built of struts, cables, and springs where the two halves connect at midspan (Motro et al. 2006)(Rhode-Barbarigos et al. 2012).

The deployment path of this tensegrity structure is rarely the same when repeating deployment-folding cycles using the same control commands (Veuve et al. 2015)(Sultan 2014)(Aldrich and Skelton 2003). Incorporating biomimetic behavior (mimicry of natural processes) such as learning and self-diagnosis has potential to enhance behavior of the structure (Adam and Smith 2007)(Cully et al. 2015)(Lobo and Vico 2010). Such enhancement is most effective when accurate simulations of behavior are available.

Continuous cables connect at mid-span nodes are secured at the supports by motors that rotate a drum of cable in order lengthen or shorten cables. These cables are installed with a helical twist along the length of the structure and guided by cable seats on joints. Since continuous cables are able to slide over joints, cable-friction forces may influence movement. This effect has been studied for mechanical limbs with tendons (Ijspeert 2014) as well as in the context of sliding roofs (Hongbo and Zhihua 2012). Another example of sliding cables for robotic applications includes a prototype robotic hand (Borghesan et al. 2011)(Palli and Melchiorri 2014). Cables acting as tendons lengthen and retract to control the angle at a joint.

Friction phenomena include static friction and kinetic friction effects (Amontons 1702)(Wit et al. 1995). Except for a self-locking joint (Ding and Li 2015)(Li et al. 2013) and a deformable joint structure called the FAST mast (Stohlman and Pellegrino 2010), simulations of deployable and adaptive structures have not explicitly accounted for friction effects. Vadivuchezhian et al. (2011) discussed the evolution of friction coefficients at micro levels and the behavior of contact surfaces that are different for the Coulomb friction (simplification that contact area increases linearly with increased normal force). Vadivuschezhian was only able to observe non-Coulomb behavior; no parameterization and classification of the friction force behavior was attempted.

Some truss roof designs have included sliding cables to guide the installation or operability (Hincz 2009). Vectors formed by the angles of the cable around the pulleys determined the resulting force and the friction contribution of the pulley. Similar concepts were used to calculate belt friction (Lima and Sampaio 2015)(Wang et al. 2015).

When a cable is wrapped around a pulley, the normal force is perpendicular to the midpoint of the pulley contact. Friction forces are aligned with the cable orientation and this has lead to studies of incremental loss due to friction along the contact length (Wang et al. 2015). Although these studies have taken friction effects into account, they did not investigate how friction influenced movement of the structure.

Recent simulations of tensegrity structures have employed the method of dynamic relaxation (DR) with kinetic damping, a static analysis that has been used for decades in the design of tent structures and cable stayed bridges (Barnes et al. 2013)(Bel Hadj Ali et al. 2011). This method has also been used to simulate the behavior of adaptive tensegrity structures (Fest et al. 2004)(Domer and Smith 2005)(Sultan and Skelton 2003)(Korkmaz 2011)(Kmet et al. 2012). These structures are held in a state of self-stress; otherwise the structure is unstable due to mechanisms (Schenk et al. 2007). Self-stress is introduced by controlled elements, such as continuous cables. Forces in all segments of each continuous cable have been assumed to be equal (Bel Hadj Ali et al. 2012)(Veuve et al. 2015). Assessment of the member forces in continuous elements caused by friction has not been carried out.

The overall goal of this work is to enhance DR simulations through use of an experimental setup that helps study friction behavior at the nodes of a deployable tensegrity structure. The structure is a topology that could be used as a footbridge (Rhode-Barbarigos et al. 2010). This objective leads to several tasks. Firstly, it is determined whether or not friction force is a significant contributor to the behavior of the structure. Then, the identification and prioritization of the parameters that affect the friction force are carried out. A comparison of static and kinetic behavior of the tensegrity structure is performed. Lastly, with the inclusion of friction in the simulation, critical elements are identified.

The paper begins with an experimental-setup section that describes the assembly and data collection for the friction test and the tensegrity structure. A preliminary analysis of the friction-test results characterizes coefficients of static and kinetic friction with respect to cable tension using two methods (approximate and segment) for calculating friction forces. In the following section, the paper focuses on results from testing a near-full-scale tensegrity structure in the laboratory. Comparisons of the friction test and tensegrity folding test are performed. Finally, dynamic relaxation analysis with and without friction effects are compared in terms of deflection and member forces.

FRICTION-TEST SETUP

Simulations of the tensegrity structure are not in full agreement with measured behavior. Simplifications such as dimensionless joints and frictionless cables are a major contribution to this discrepancy. Friction tests involved running a single cable over a joint and sliding cables on a deployable 1/4-scale tensegrity structure.

Since friction forces are dependent on the applied normal force, the friction test provides information on the behavior of continuous cables for a range of normal forces. Normal forces originate from cable tension and interior angles formed by the cable that is bent over the joint.

A relationship between the coefficient of friction and normal force at the joint needs to be incorporated into simulation of the tensegrity structure. The two types of friction, static and kinetic, are shown schematically in Fig. 1. Static friction is the maximum value of friction force before movement occurs. It is used to calculate the static coefficient of friction. The kinetic friction force value is the unlubricated friction force when the system is in motion. This value is used to calculate the kinetic coefficient of friction (Shaw 1966). In Fig. 1, the friction force value, F_f, is normalized by the maximum friction force, $F_{f(max)}$, value for each trial.

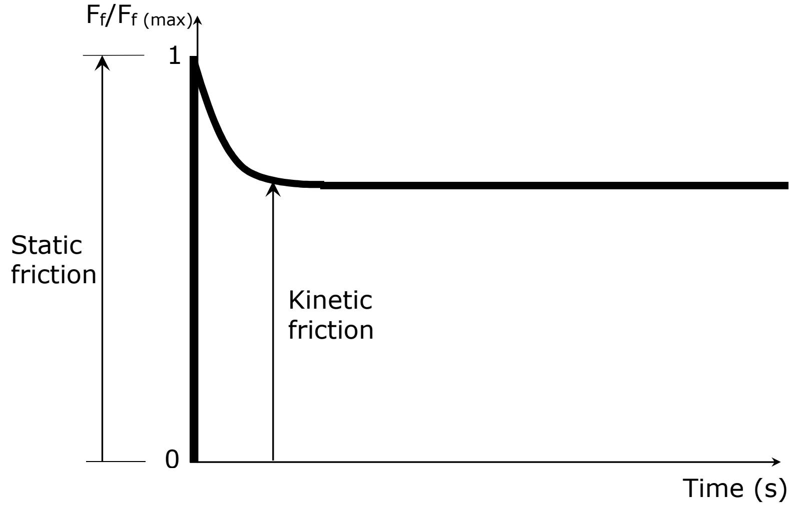

FIG. 1: Schema of normalized friction force behavior for materials exhibiting static and kinetic friction from the beginning of sliding

The friction test isolated the effect of a braided steel cable passing over the cable seat in an identical way to those found on the 1/4-scale structure (Fig. 2) (Rhode-Barbarigos et al. 2010). The setup included a steel rod with a joint seat and plastic tube for a 4 mm diameter steel cable. All materials were identical to those on the tensegrity structure. At the base of the rod was a strain rosette that measured bending strains caused by cable sliding. There was a 5 mm high widening at the base of the steel rod for connection purposes. Since the rosette was 12 mm from the base, it was away from the influence of stress concentrations. A basket containing masses of 50 kg to 150 kg in equal amounts was attached at each end of the cables. The interior angle of the cable varied from 117 ° to 170 °.

Nearly frictionless 120 mm ∅ pulleys at 400 mm center-to-center on either side of a center rod with the joint seat helped create the interior cable angles observed on the structure. With adjustable heights, the center column formed interior angles representative of those measured on the tensegrity structure. A 150 mm long and 15 mm ∅ steel rod holding the steel joint seat was bolted into the height-adjustable column. At the base of the steel rod, a strain rosette of four HBM LY41 350 $\Omega \pm 0.35$ % strain gauges were installed to measure the bending of the rod. The cable seat had a double curvature and is lined with a plastic tubing. Therefore, friction interface was a 4 mm ∅ braided steel cable sliding on medium-density polyethylene. Data acquisition for these tests used an HBM QuantumX MX1615B

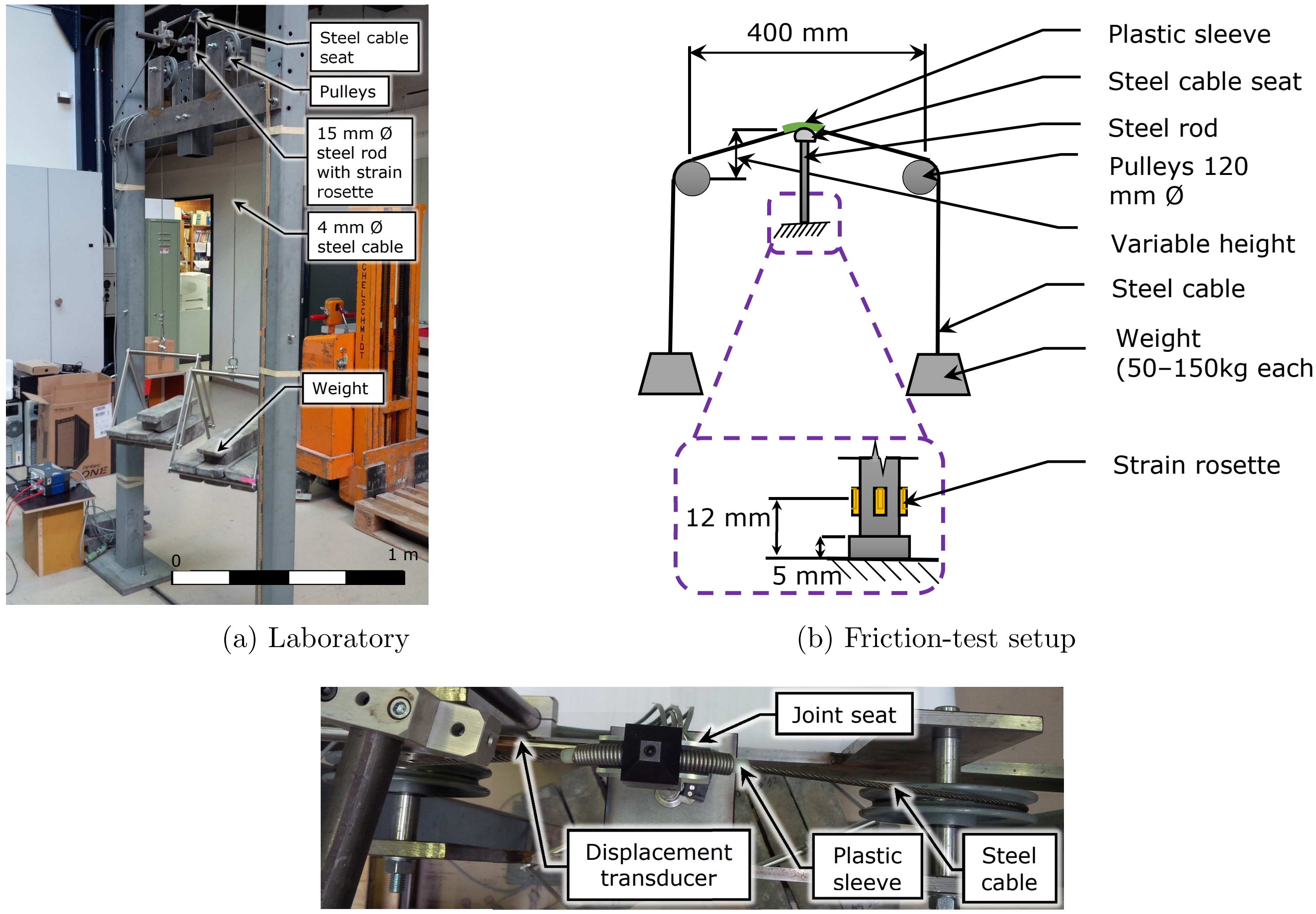

(a) Laboratory

(b) Friction-test setup

(c) View from above of friction-test setup

FIG. 2: Laboratory photo (a), schematic (b) of friction-test setup (not to scale), and view of joint from above (c)

device and National Instruments MAX software for data collection. Each cable angle and weight test was repeated twenty times. The maximum standard deviation of the tension force measured in the cables per set of tests was approximately 20 N.

As one basket was loaded with additional weights from 0.3 kg to 2.0 kg, the static coefficient of friction was overcome and caused the cable to slide over the joint, thus bending the rod. With the horizontal movement of the joint seat, friction force was determined through measuring strains at the base of the rod.

Fig. 3 shows the joint seat and the position of the displacement transducer. The plastic sleeve has been chosen to reduce friction effects. The displacement transducer had a maximum stroke of 50 mm. Preliminary calculations have determined that, given the loading and the cross-sectional properties of the rod, deflections do not exceed the limit of either the displacement transducer or the elastic properties of the material.

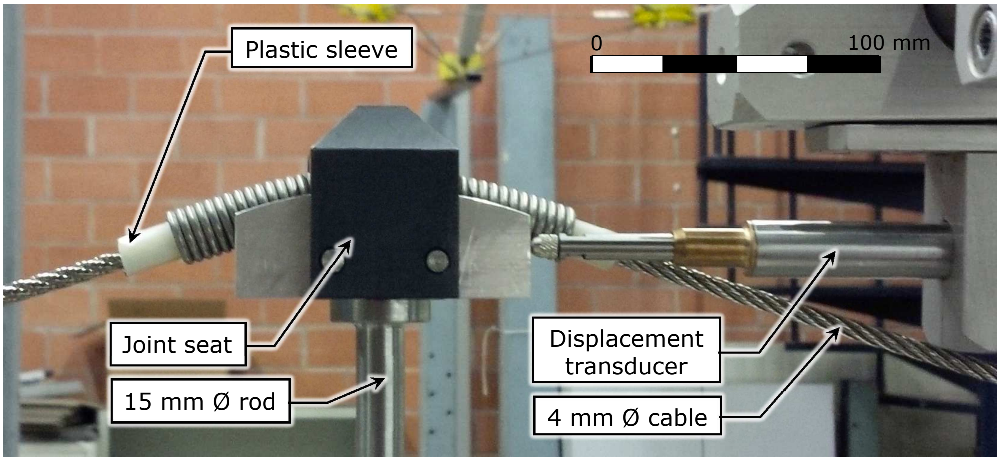

FIG. 3: Horizontal displacement measured at the joint

Approximate method

The diagram in Fig. 4 shows the interaction of the cable on the joint seat and the variables used to determine friction with the approximate method. Values of static and kinetic friction were selected from the tests using the peak and the steady-state friction force respectively. The coefficient of friction, μ, is a ratio of the friction force to the normal force and this is used to compare the results from each cable angle, and each cable tension. Friction forces were normalized by the interior angle (θ) formed by the cable at the joint. The tension value for the element in the opposite direction of motion T_1 and the tension value for the element in the direction of motion is T.

The measurement of horizontal movement of the joint seat is needed to determine friction F_f. The normal force, F_n, only contributes to the bending moment of the system when there is deflection in the steel rod. With the horizontal movement of the joint seat, friction, F_f, is quantified using a summation of moments and strain measurements at the base of the rod. For the purposes of this paper, this is called the approximate method.

Using this test, a range of probable tension forces and cable angles are examined. Table 1 contains the matrix showing values of test parameters. The cable tensions and interior angles of the cable at the joint cover the range of possible values that are observed during deployment and folding of the tensegrity. Results from these tests help quantify possible

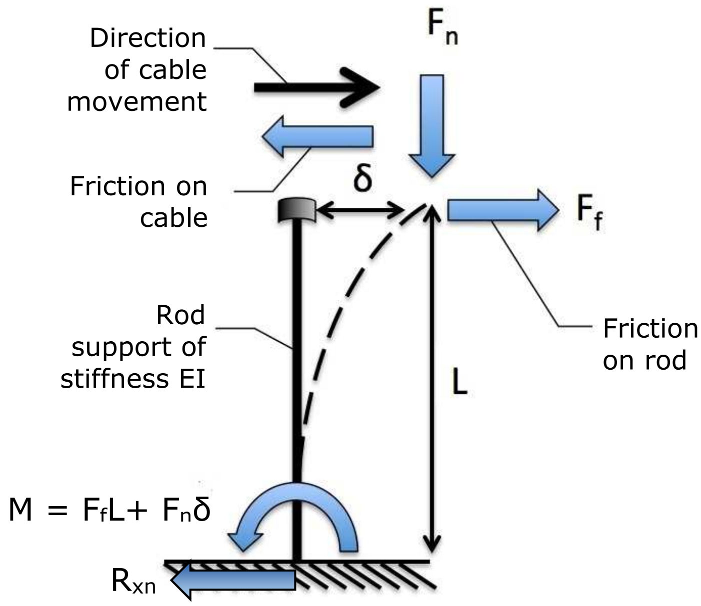

FIG. 4: Force diagram acting on rod for the approximate method

friction forces that act on the tensegrity structure.

Cable Angle θ (°)	Cable Tension (kN)
117	1, 1.5, 2, 2.5, 3
146	1, 1.5, 2, 2.5, 3
170	1.5, 2, 2.5, 3

TABLE 1: Test matrix of cable angle and tension

Segment method

The segment method for calculating friction forces involves discretization of the contact surface length of the cable and the joint seat into segments (Fig. 5). This development is adapted from Lubarda (2014). Arc angle $\Delta\theta$ is the discretized interior angle that the cable forms over the contact surface. When the discretized cable length is short, the contact is assumed to be linear.

A summation of the forces in x and y produces Equations (1) and (2).

$$\sum F_x = 0 \\ = T\cos\left(\frac{\Delta\theta}{2}\right) + \mu\Delta N - (T+\Delta T)\cos\left(\frac{\Delta\theta}{2}\right) \tag{1}$$

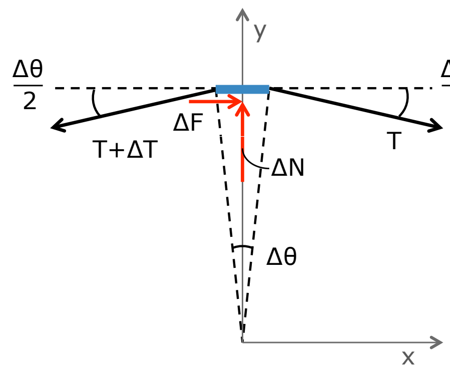

FIG. 5: Force diagram for the segment method

$$\begin{aligned}\sum F_y &= 0 \\ &= \Delta N - (T + \Delta T)\sin\left(\frac{\Delta\theta}{2}\right) - T\sin\left(\frac{\Delta\theta}{2}\right)\end{aligned} \tag{2}$$

When $\frac{\Delta\theta}{2}$ describes the angle of an infinitesimally small angle segment, the small angle assumption is applicable, $\sin\left(\frac{\Delta\theta}{2}\right) = \frac{\Delta\theta}{2}$ and $\cos\left(\frac{\Delta\theta}{2}\right) = 1$. Substitution yields Equation (3).

$$\begin{aligned}\sum F_x &\Rightarrow \Delta T = \mu\Delta N \\ \sum F_y &\Rightarrow \Delta N = T\Delta\theta\end{aligned} \tag{3}$$

The above set of equations simplifies to a single relationship (4).

$$\Delta T = \mu T \Delta\theta \tag{4}$$

For the change in tension over the entire contact surface, Equation (4), is integrated over θ.

$$\int_{T_1}^{T_2} \frac{dT}{T} = \mu \int_0^{\theta} d\theta \tag{5}$$

Lastly, this simplifies to the following:

$$T_1 = T e^{\mu\theta} \tag{6}$$

The friction force is tangential to each segment. The summation of these segments results in the total friction value, F_f. For the purposes of this paper, this is called the segment method for calculating friction effects at joints. Fig. 6 shows joint equilibrium for the DR analysis that has been extended to include the effect of friction.

To experimentally determine the coefficient of friction, the segment method employs the angle of the cable at the joint θ and tension values T and T_1, see subsection "Determination of the coefficient of friction". This coefficient value is then used in the DR analysis along with calculated values of θ and T to determine the value of T_1, see subsection "Implementation of friction in dynamic relaxation analysis" below.

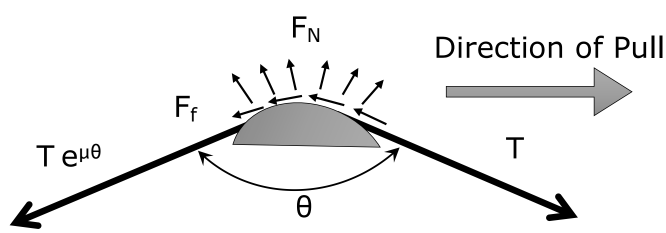

FIG. 6: New joint equilibrium diagram for modified dynamic-relaxation analysis. Cable angle = θ

RESULTS - FRICTION-TEST SETUP

The following sections contain observations related to laboratory experiments using the setup described in Fig. 2.

Experiments

Fig. 7 shows friction force behavior with respect to time for a constant load on the friction-test setup. When the load is added, the friction force reaches a peak, called break friction, before the system is in motion. As soon as the system begins to move, the friction force drops non-linearly by a value called Stribeck friction. Lastly, the system moves into a steady-state kinetic friction, a value called Coulomb friction. Observation of this relationship is common to all tests of the friction-test setup and are in agreement with the relationship of Fig. 1. Since the difference between kinetic and static friction force is small and therefore, values of kinetic friction are adopted as global structural values.

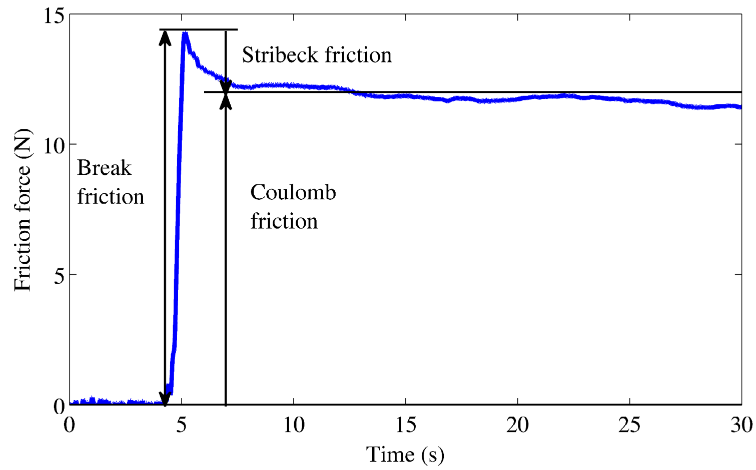

FIG. 7: Example friction-time relationship for a friction test having a cable tension of 2 kN at an angle of 146 $^{\circ}$

Determination of the coefficient of friction

Results from the friction-test setup confirmed the hypothesis that friction is non-negligible and thus the coefficient of friction has been determined. The approximate method provides a solution for the equilibrium equation of the forces acting on the rod using bending moments from a strain rosette. The segment method uses the evaluation of forces on an elemental segment of cable.

Fig. 8a and Fig. 8b show the coefficients of static and kinetic friction based on interior angle and cable tension using the approximate method. Fig. 8c and Fig. 8d show the coefficients of static and kinetic friction for the segment method determined by an elemental equilibrium of forces T and T_1 at the joint using Equation 6. Similarity evaluation using the Student t-test accepted the null hypothesis that there is not a significant difference between static and kinetic coefficients of friction at a 95% confidence interval for results using both methods.

The relationship between the coefficient of friction and cable tension per degree of interior cable angle does not change significantly throughout the set of plots. As the interior angle decreases, the coefficient of friction increases. Purely Coulomb behavior would not show change of friction coefficient with respect to normal force. Coulomb friction does not adequately describe behavior when normal forces are low ($\theta = 170°$). The segment method

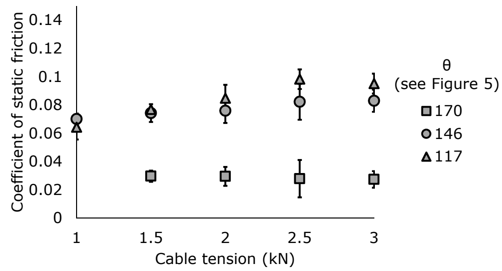

(a) Approximate method: Static friction

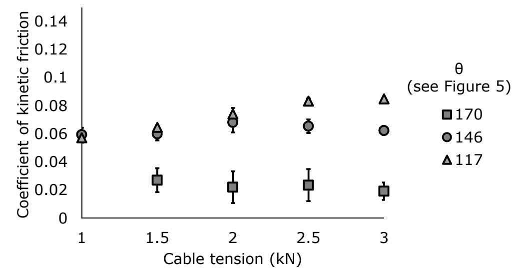

(b) Approximate method: Kinetic friction

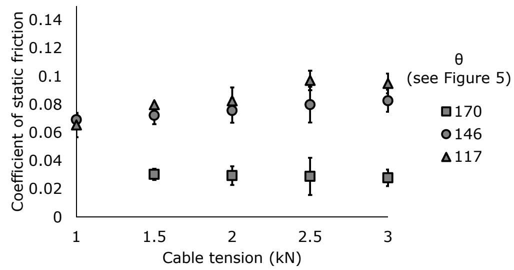

(c) Segment method: Static friction

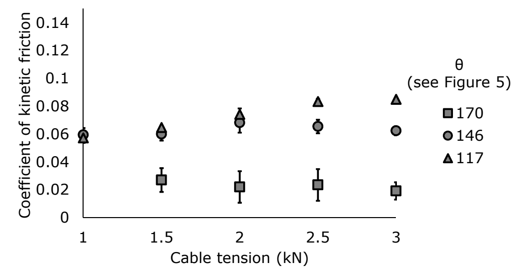

(d) Segment method: Kinetic friction

FIG. 8: Static and kinetic friction for the approximate method (a and b) and the segment method (c and d) for fives values of cable tension and three angles of θ. Each point is the mean of ten tests. The bars at each point are drawn at 2 standard deviations.

is most easily integrated into dynamic-relaxation simulations.

Comparison between approximate method and segment method

The results using the approximate method support the results obtained by the segment method. At 95% confidence, both methods provide similar results. Since the segment method is more easily implemented in simulations, it is adopted in the next section to modify the dynamic-relaxation analysis. The effective coefficient of friction decreases as the internal angle increases towards 180 $^\circ$ (flat) since there is minimal force on the joint seat.

Tests with an internal angle of 117 $^\circ$ had the greatest increase in friction coefficient as tension increased. Since the maximum difference in the friction coefficients for the 117 $^\circ$ tests is small (approximately 0.03), tests for every interior angle are assumed to have no effect on the friction coefficient as tension increases. Therefore, coefficients of static and kinetic friction are dependent only on the interior angle of the cable at the joint. Additionally, the segment method accurately describes the behavior while requiring less information, cable tension and interior angle, than the approximate method, which requires the additional information of rod properties, strain values, and horizontal displacement.

RESULTS - TENSEGRITY STRUCTURE TESTS AND SIMULATIONS

Cable friction tests were conducted on one half of the tensegrity structure in order to apply concepts learned from the friction tests. The 1/4-scale structure is a 4 m long pentagonal shape built in two halves of two modules each. Each half is composed of fifteen springs, five continuous cables, thirty struts, and twenty non-continuous struts (Fig. 9).

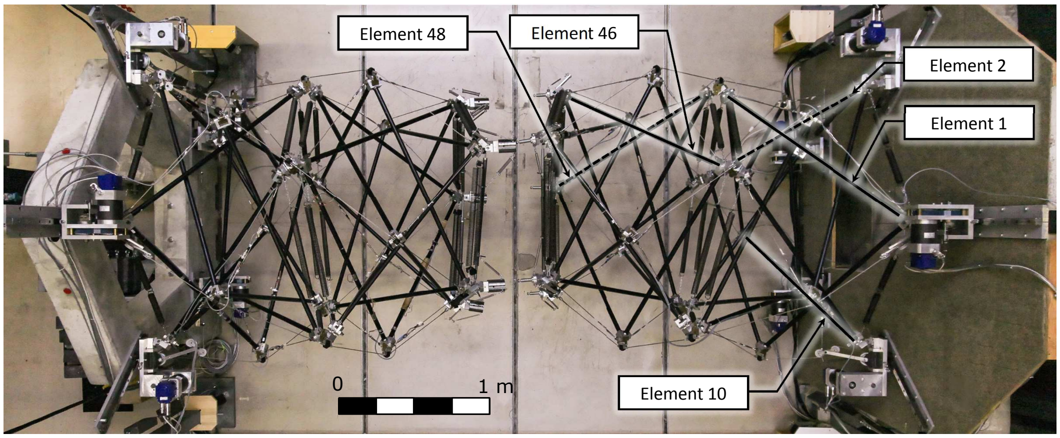

FIG. 9: Top view of 1/4-scale tensegrity footbridge during deployment just prior to midpsan connection

Struts are 28 mm diameter hollow steel tubes and cables are steel braided 4 mm nominal diameter. Continuous cables connect at mid-span nodes, pass over joints of the structure, and are secured at the supports by the motors that control their length. Continuous cables allow for controlled folding and deployment of the structure. Movement of the structure is slow enough to exclude dynamic effects and therefore, the static method of DR can be implemented.

Tests on the tensegrity structure involved control commands that were limited to the shortening and lengthening of continuous cables by 5 cm. Although the laboratory structure does not have a deck and other parts, the shape of this structure has been identified as a possible design for a footbridge (Rhode-Barbarigos et al. 2010) shown in elevation view and cross section view in Fig. 10). Pedestrians walk in the center of what has been called a ”hollow-rope” structure (Motro et al. 2006).

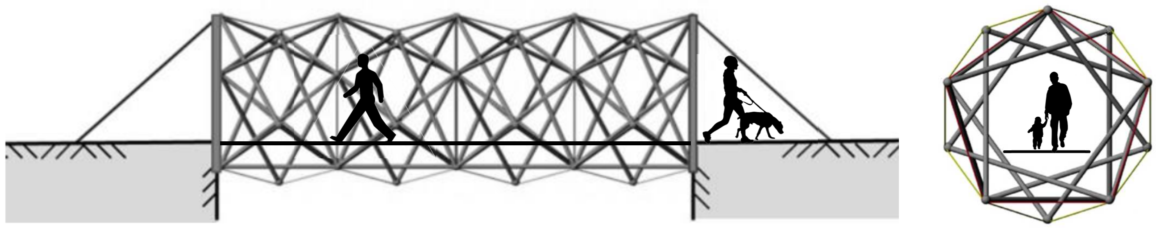

(a) Elevation view (b) Cross-section view

FIG. 10: Elevation view (a) and cross-section view (b) of a "hollow-rope" tensegrity footbridge

Implementation of friction in dynamic relaxation analysis

When the DR analysis was adapted for continuous cables (Bel Hadj Ali et al. 2011), the assumption was made that each segment of the continuous cable had the same tension. Magnitude and direction of the friction force were added to the analysis to ensure convergence included the friction component (see Fig. 6). Friction force is added to the cable opposing the direction of motion.

Fig. 11 shows the effect of including friction in the simulation on an elevation view of one half of the structure. The tensegrity structure does not deploy as far when friction is included in the simulation. This affects the values of control commands that are needed for midspan connection (Veuve et al. 2015).

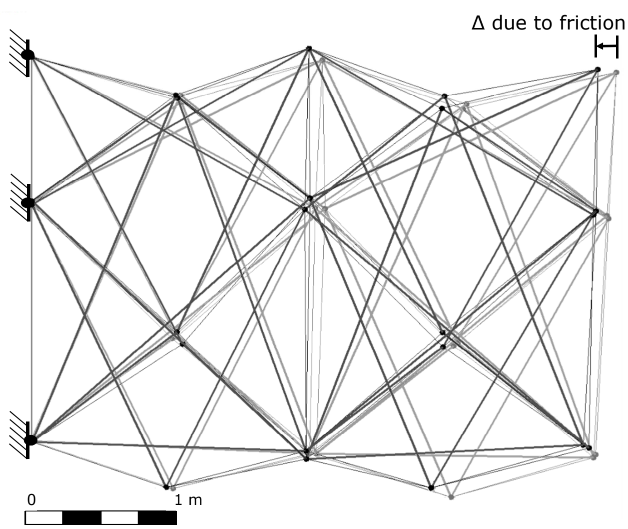

FIG. 11: Elevation view of deflected position simulated under self-weight showing the difference in calculations with (grey) and without (black) friction

Connection at midspan occurs between nodes with a rod on one connecting node and cone connection on the other. The cone has a 30 mm radius and thus an allowable discrepancy between nodes of ±30 mm. This value was fixed through previous research (Veuve et al. 2015). The distance between each node for the friction and frictionless simulations of DR are presented as ΔL in Table 2. Although the change of end node position of the deployed structure is small, it is not negligible compared with a 30 mm allowable discrepancy. When both bridge halves are actuated, each bridge half should have a maximum discrepancy of 30 mm.

Node	Δ L (mm)	% of 30 mm discrepancy
1	2.0	6.8
2	2.3	7.7
3	3.5	11.8
4	3.6	12.0
5	3.0	9.9

TABLE 2: End node position change due to inclusion of friction effects in dynamic relaxation analysis

When comparing forces (Fig. 12), differences are limited to those above 0.05 kN since there were two types of member-force data. Even at ideal pre-stress states, forces in some members are low; presenting relative changes is not meaningful. Forces in the continuous cables change minimally in simulation when the friction component is integrated. Discontinuous cables are moderately affected by the model modification and the struts were the most affected.

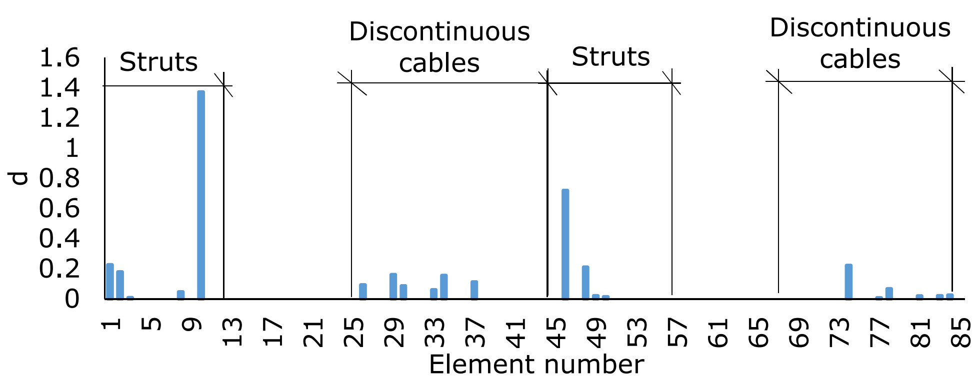

FIG. 12: Relative difference, d, between dynamic-relaxation simulations with and without friction. Results are shown only when member forces are greater than 0.5 kN

Measurements during deployment

The installation of a HBM U2A in-line 10 kN load cell on the continuous cable at the midspan joint is shown in Fig. 13. Data acquisition was completed used an HBM QuantumX MX840 device and National Instruments MAX software for data collection. The test was repeated twenty times for cable actuations of 1 cm, 5 cm, 10 cm, and 40 cm. Amongst the cable actuation tests, mean axial forces in the five continuous cables varied from 400 N to 700 N. For the same cable actuation, there was a maximum standard deviation of axial force of 150 N and an average standard deviation of 7.0 N. The effect of friction on a cable depends on the direction of the deployment-folding cycle.

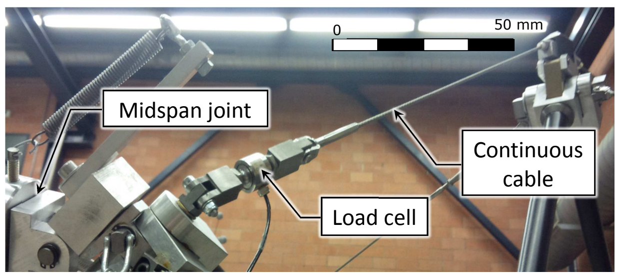

FIG. 13: Continuous cables equipped with load cells on tensegrity structure

In order to further compare results between friction and tensegrity structure tests, deployment and folding cycles were conducted for the tensegrity structure and the friction-test setup. A sample of normalized friction force and cable length change for the friction-test setup and the tensegrity structure are presented in Fig. 14. This figure shows measurements from the friction test (Fig. 2), measurements from the tensegrity structure, and linearization of tensegrity structure measurements. The horizontal axis is the normalized horizontal displacement of deployment and the vertical axis is the normalized force. The dotted line is a data sample from a 5 cm cable actuation on the tensegrity structure. It has been normalized by the maximum distance moved and the maximum axial force measured. The solid line is a linear regression of this sample data using least squares with a correlation coefficient of approximately 0.76. The dashed line represented the normalized average of the friction-test setup for 146° and cable tension of 2 kN. Even though the length change of the cable was not the same for the two experimental setups, the regression slopes are similar.

Much more variation and non-linearity occurs in the tensegrity structure. Since force per

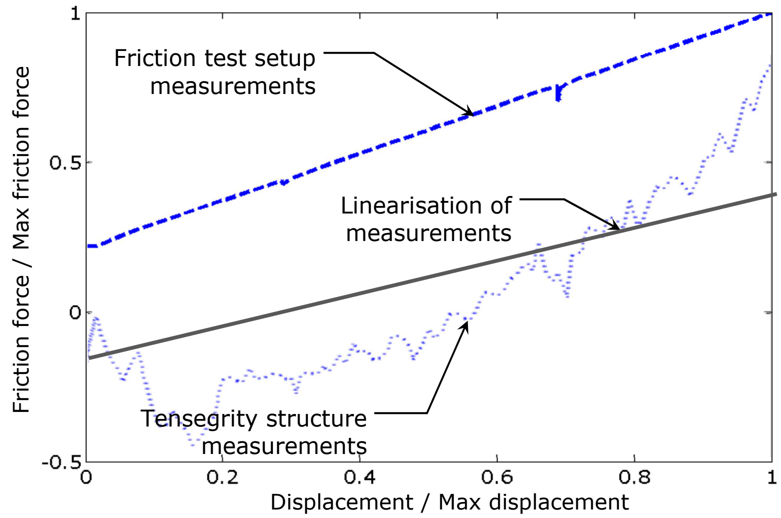

FIG. 14: Sample measurement data: normalized friction force and displacement relationship for friction test and tensegrity structure

unit deflection is a measure of the stiffness of the tensegrity structure, the effective stiffness of both experimental setups are similar. Therefore, conclusions drawn from the friction-test setup are applicable to the tensegrity structure.

There is much variability in the deployment of the tensegrity structure that cannot be accounted for by friction effects. Friction is a relatively constant influence on deployment and therefore, other factors contribute to irreproducible movement. For example, construction details of the structure, particularly the joints, have important influence on the behavior.

Comparing simulations with measurement data

Friction effects are approximated to be those related to static behavior since cables on the tensegrity structure are actuated at low-velocity. When friction behavior is included in tensegrity structure simulations, the sources of differences between simulation and test results are largely limited to those related to joint behavior.

Simulations of the structure folding with 5 cm of cable retraction were run with and without including friction effects. Simulated axial forces on the continuous cables were compared with measurements taken from the tensegrity structure. Measurement data was filtered to match the twenty simulated actuation steps.

Differences between simulation and measurement for each actuation step have been evaluated for cases with and without friction effects. The simulation with friction effects has a mean difference from measurements of 50% less than the simulation without friction. Additionally, the standard deviations for simulations with friction are on average 40% less than simulations without friction effects.

Four continuous cable elements on one bridge half have been instrumented with load cells (Fig. 15). Fig. 16 shows the average tension during a 5 cm deployment in these elements for simulation without friction, simulation with friction, and measurement data. The horizontal axis shows the instrumented continuous cables and the vertical axis shows the average tension values [kN]. Including friction of the continuous cables during deployment reduces the difference between simulation and measurement data. As mentioned earlier other factors, such as joint movements, contribute to the remaining differences.

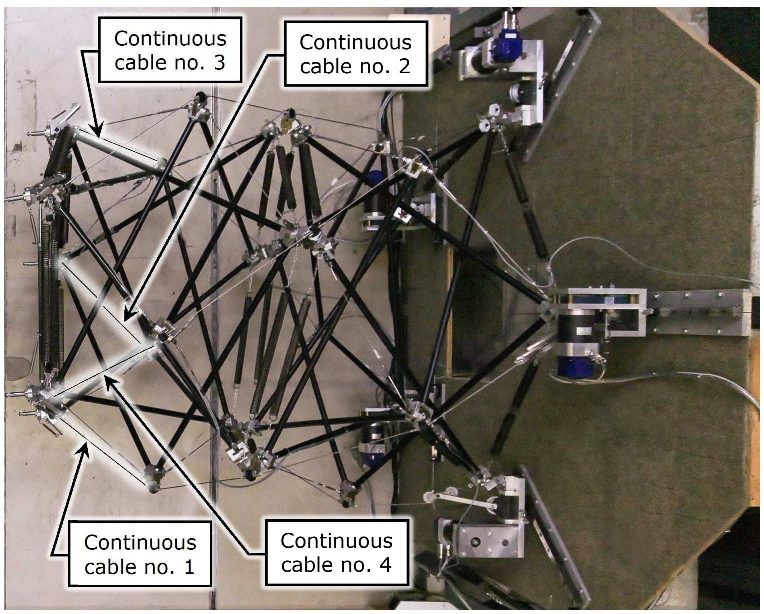

FIG. 15: Top view of one half of deployed 1/4-scale tensegrity footbridge. Continuous cables instrumented with load cells are labelled

CONCLUSIONS

Friction force needs to be taken into account when modeling deployment behavior. Since the effective coefficient of friction is not constant, the interior cable angle is the best parameter to describe variability. Static and kinetic friction forces are adequately combined into one calculation. The segment method is most easily integrated into dynamic-relaxation simulations. Including friction of the continuous cables during deployment reduces the difference

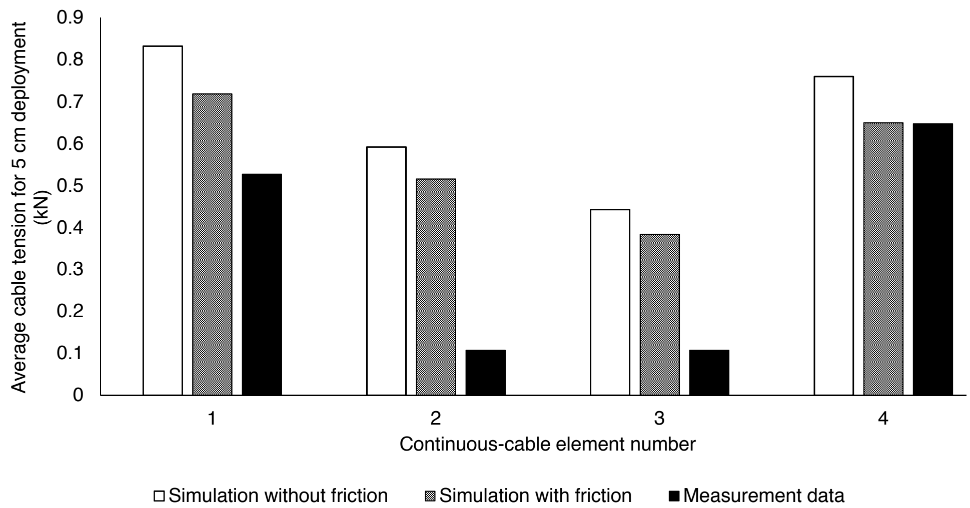

FIG. 16: Average tension values for simulation without friction, simulation with friction, and measurement data for 5 cm deployment

between simulation and measurement data. Strut elements of the tensegrity structure are most critically affected by friction. Lastly, strut elements are most influenced by friction. Further work will involve modeling joint behavior and studying dependence of cable angle on the effective coefficient of friction.

ACKNOWLEDGEMENTS

The research is sponsored by the Swiss National Science Foundation under project number 20020_144305. The authors wish to express thanks to N. Bel Hadj Ali, J.F. Molinari, and N. Veuve for fruitful discussions and S. Despont with the design of the friction test.

REFERENCES

Adam, B. and Smith, I. F. C. (2007). “Self-Diagnosis and Self-Repair of an Active Tensegrity Structure.” *Journal of Structural Engineering*, 133(12), 1752–1761.

Aldrich, J. B. and Skelton, R. E. (2003). “Control/structure optimization approach for minimum-time reconfiguration of tensegrity systems.” *Smart Structures and Materials*, 5049(7), 448–459.

Amontons, G. (1702). “De la résistance causée dans les machines, tant par les frottemens des parties qui les composent, que par la roideur des cordes qu’on y employe, et la maniere de calculer l’un et l’autre.” *Histoire de l’Académie Royale des Sciences 1699, Paris*, 206.

Barnes, M. R., Adriaenssens, S., and Krupka, M. (2013). "A novel torsion/bending element for dynamic relaxation modeling." *Computers & Structures*, 119(12), 60–67.

Bel Hadj Ali, N., Motro, R., and Smith, I. F. C. (2012). "Design Aspects of a Deployable tensegrity-hollow rope footbridge." *International Journal of Space Structures*, 27(2), 81–95.

Bel Hadj Ali, N., Rhode-Barbarigos, L., and Smith, I. F. C. (2011). "Analysis of clustered tensegrity structures using a modified dynamic relaxation algorithm." *International Journal of Solids and Structures*, 48(5), 637–647.

Borghesan, G., Palli, G., and Melchiorri, C. (2011). "Friction compensation and virtual force sensing for robotic hands." *Proceedings - IEEE International Conference on Robotics and Automation, Shanghai, China*, 4756–4761.

Cully, A., Clune, J., Tarapore, D., and Mouret, J.-B. (2015). "Robots that can adapt like animals." *Nature*, 521(7553), 503–507.

Ding, X. and Li, X. (2015). "Design of a type of deployable/retractable mechanism using friction self-locking joint units." *Mechanism and Machine Theory*, 92, 273–288.

Domer, B. and Smith, I. F. C. (2005). "An Active Structure that Learns." *Journal of Computing in Civil Engineering*, 19(1), 16–24.

Fest, E., Shea, K., and Smith, I. F. C. (2004). "Active Tensegrity Structure." *Journal of Structural Engineering*, 130(10), 1454–1465.

Gantes, C. J., Connor, J. J., Logcher, R. D., and Rosenfeld, Y. (1989). "Structural analysis and design of deployable structures." *Computers and Structures*, 32(3-4), 661–669.

Hincz, K. (2009). "Nonlinear Analysis of Cable Net Structures Suspended From Arches with Block and Tackle Suspension System, Taking into Account the Friction of the Pulleys." *International Journal of Space Structures*, 24(3), 143–152.

Hongbo, L. and Zhihua, C. (2012). "Influence of Cable Sliding on the Stability of Suspendome with Stacked Arches Structures." *Advanced Steel Construction*, 8(1), 54–70.

Ijspeert, A. J. (2014). "Biorobotics: using robots to emulate and investigate agile locomotion.." *Science (New York, N.Y.)*, 346(6206), 196–203.

Kmet, S., Platko, P., and Mojdis, M. (2012). "Analysis of Adaptive Light-Weight Structures." *Procedia Engineering*, 40(7), 199–204.

Korkmaz, S. (2011). "A review of active structural control: challenges for engineering informatics." *Computers & Structures*, 89(23-24), 2113–2132.

Li, J., Yan, S., Guo, F., and Guo, P. (2013). "Effects of damping, friction, gravity, and flexibility on the dynamic performance of a deployable mechanism with clearance." 227(8), 1791–1803.

Lima, R. and Sampaio, R. (2015). "Stick-mode duration of a dry-friction oscillator with an uncertain model." *Journal of Sound and Vibration*, 353(5), 259–271.

Lobo, D. and Vico, F. (2010). "Evolutionary development of tensegrity structures.." *Bio Systems*, 101(3), 167–76.

Lubarda, V. a. (2014). "The mechanics of belt friction revisited." *International Journal of Mechanical Engineering Education*, 42(2), 97–112.

Motro, R. (2011). "Structural morphology of tensegrity systems." *Meccanica*, 46(1), 27–40.

Motro, R., Maurin, B., and Silvestri, C. (2006). "Tensegrity rings and the hollow rope." *IASS Symposium, New Olympics, New Shells and Spatial Structures*, Beijing, China.

Palli, G. and Melchiorri, C. (2014). "Friction compensation techniques for tendon-driven robotic hands." *Mechatronics*, 24(2), 108–117.

Pellegrino, S. (2001). *Deployable Structures*. Springer, Vienna.

Pellegrino, S. and Calladine, C. (1986). "Matrix analysis of statically and kinematically indeterminate frameworks." *International Journal Solids Structures*, 22(4), 409–428.

Rhode-Barbarigos, L., Bel Hadj Ali, N., Motro, R., and Smith, I. F. (2010). "Designing tensegrity modules for pedestrian bridges." *Engineering Structures*, 32(4), 1158–1167.

Rhode-Barbarigos, L., Schulin, C., Bel Hadj Ali, N., Motro, R., and Smith, I. F. C. (2012). "Mechanism-based approach for the deployment of a tensegrity-ring module." *Journal of Structural Engineering*, 138(4), 1–12.

Schenk, M., Guest, S., and Herder, J. (2007). "Zero stiffness tensegrity structures." *International Journal of Solids and Structures*, 44(20), 6569–6583.

Shaw, M. C. (1966). *Metal cutting principles*, Vol. 1. Oxford University Press, New York.

Snelson, L. (1996). "The art of tensegrity." *International Journal of Space Structures*, 11(1-

2), 43–48.

Stohlman, O. and Pellegrino, S. (2010). “Shape accuracy of a joint-dominated deployable mast.” *Collection of Technical Papers - AIAA/ASME/ASCE/AHS/ASC Structures, Structural Dynamics and Materials Conference, Orlando, Florida, USA*, 1–15.

Sultan, C. (2014). “Tensegrity deployment using infinitesimal mechanisms.” *International Journal of Solids and Structures*, 51(21-22), 3653–3668.

Sultan, C. and Skelton, R. (2003). “Deployment of tensegrity structures.” *International Journal of Solids and Structures*, 40(18), 4637–4657.

Vadivuchezhian, K., Sundar, S., and Murthy, H. (2011). “Effect of variable friction coefficient on contact tractions.” *Tribology International*, 44(11), 1433–1442.

Veuve, N., Safaei, S. D., and Smith, I. F. C. (2015). “Deployment of a Tensegrity Footbridge.” *Journal of Structural Engineering*, 141(11), 1–8.

Wang, D., Zhang, D., Mao, X., Peng, Y., and Ge, S. (2015). “Dynamic friction transmission and creep characteristics between hoisting rope and friction lining.” *Engineering Failure Analysis*, 57(10), 499–510.

Wit, C. C. D., Olsson, H., Member, S., J, K., Lischinsky, P., Canudas De Wit, C., and Aström, K. J. (1995). “A new model for control of systems with friction.” *IEEE transactions on automatic control*, 40(3), 419–425.